INVITED ARTICLE

Densification of ZrB_2–SiC nanocomposites prepared using $ZrSi_2$, B_4C, and C additives

Sea-Hoon Lee,[a),b)] Lun Feng,[b)] and Chang Jun Bae
Engineering Ceramics Research Group, Korea Institute of Materials Science (KIMS), Changwon, Gyeongnam 641-831, Republic of Korea

(Received 30 December 2016; accepted 18 May 2017)

Dense ZrB_2–SiC nanocomposites were fabricated at 1450 °C by the high-energy ball milling (HEBM) of ZrB_2 powder with $ZrSi_2$–B_4C–C additives and reactive spark plasma sintering (R-SPS). The sizes of ZrB_2 and SiC grains were 80–350 nm, and the phases were homogeneously distributed because of the molecular-level homogeneity of the constituents in $ZrSi_2$ and the homogeneous mixing of the raw powders by HEBM. The deformation of $ZrSi_2$ or the reactions between the additives during R-SPS did not strongly promote the densification. Fine and homogeneously distributed ZrB_2 and SiC particles formed by HEBM and R-SPS were the major reasons for the low temperature densification. The fine particles which had high surface energy provided the driving force for densification at low temperatures. Also, the fine SiC grains suppressed the growth of ZrB_2 grains during densification. The 4-point bending strength of the composites sintered at 1500 °C was 354 MPa.

I. INTRODUCTION

ZrB_2 has attracted attention in recent years because of its high melting temperature (>3200 °C), excellent oxidation resistance above 1800 °C, relatively low density (6.09 g/cm^3), high strength (500–1000 MPa), and moderate fracture toughness (2.5–4.5 MPa m$^{1/2}$).[1,2] As a consequence, researches have been performed for producing ZrB_2 ceramics with high relative density, fine microstructure, excellent mechanical properties, and high thermal stability.[3]

However, the material has some problems such as the difficulty of densification. Because of the strong covalent bonding and low self-diffusion coefficients, pressure-assisted sintering such as hot pressing or spark plasma sintering (SPS) above 2000 °C has been required for the densification of monolithic ZrB_2 without sintering additives. As a consequence, strong grain growth deteriorated the mechanical properties of the ultra-high temperature ceramic materials (UHTC).[4]

To decrease the sintering temperature of ZrB_2–SiC, reactive hot pressing using Zr, Si, B_4C, and C has been performed. The dense ZrB_2 and ZrB_2–SiC composites were prepared without using sintering additives at 1800–1900 °C.[5,6] However, the grain sizes of the resultant products were relatively large (1–10 μm) and a careful handling of the reactive Zr metal powder in an inert atmosphere was required for the process.[7]

Reactive SPS (R-SPS) has been recently introduced to obtain UHTC with high density and a fine microstructure by using good properties such as fast heating/cooling rate, low sintering temperature, and high applicable pressure.[8,9] Wu et al. compared the grain size of ZrB_2–SiC-based composites using reactive hot pressing and R-SPS and reported that the composites prepared by R-SPS formed a more homogeneous and fine microstructure because of the fast heating rate and short holding time.[10,11]

The low temperature densification of ZrB_2 and ZrB_2–SiC has been also achieved without sintering additives by decreasing the particle size down to 9–10 nm using high-energy ball milling (HEBM) and subsequent spark plasma sintering (SPS) at 1425–1650 °C.[12–14] The sinterability of UHTC can be enhanced by HEBM due to the increase of surface area by the particle size refinement and the decrease of diffusion distance through the uniform improvement between the components.

Guo et al. densified ZrB_2 by hot pressing at 1450 °C using $ZrSi_2$ as a sintering additive.[15] The low melting temperature of $ZrSi_2$ (1620 °C) played a key role in the enhanced densification. However, the ZrB_2 densified with $ZrSi_2$ suffered from a strong decrease of strength above 1400 °C due to the softening of the additive.[16]

This problem may possibly be solved by adding B_4C and C together with $ZrSi_2$ and inducing the following reaction:

$$2ZrSi_2 + B_4C + 3C \rightarrow 2ZrB_2 + 4SiC \quad . \qquad (1)$$

$$\Delta G = -547.686 + 0.049078T \quad ,$$

Contributing Editor: Xiaowei Yin
[a)]Address all correspondence to this author.
e-mail: seahoon1@kims.re.kr
[b)]These authors contributed equally to this work.
DOI: 10.1557/jmr.2017.217

where ΔG is the Gibbs free energy (kJ/mol) and T is the temperature (°C).

During densification, $ZrSi_2$ transforms into highly refractory ZrB_2 and SiC by reaction (1) which has a minus Gibbs free energy at 20–2000 °C. Consequently, reaction (1) occurs at a low temperature if the reactants have a close contact without having oxide surface layers.

In addition to the benefit of low temperature densification and the removal of $ZrSi_2$ having low melting temperatures, the composites prepared by reaction (1) may have very fine and homogeneously intermixed ZrB_2 and SiC grains due to the molecular-level homogeneity of Zr and Si in $ZrSi_2$. The present authors reported the synthesis of homogeneously intermixed nano ZrB_2–SiC powder (20–80 nm) through reaction (1).[17]

The SiC particles promote the densification of ZrB_2 and improve the microstructure, mechanical properties, and oxidation resistance of UHTC. The SiC particles with a fine size exhibited a strong grain refining effect of the ZrB_2 matrix and excellent mechanical properties of the resultant ZrB_2–SiC ceramics.[18]

In this research, the densification of ZrB_2 using $ZrSi_2$–B_4C–C additives was performed at 1450 °C by using HEBM and R-SPS. The possible mechanisms for the low temperature densification were discussed, and some mechanical properties of the nano ZrB_2–SiC composites were analyzed.

II. EXPERIMENTAL PROCEDURE

ZrB_2 (ZrB_2–F, d_{50}: 2.12 μm, Japan New Metal Co., Osaka, Japan), $ZrSi_2$ (99.5%, <325 mesh, Alfa Aesar, Ward Hill, MA), B_4C (99%, <10 μm, Alfa Aesar), and carbon black (99.9%, d_{50}: 30 nm, Alfa Aesar) were used as starting materials. The molar ratio between $ZrSi_2$:B_4C:C was set to 2:1:3, which is the stoichiometric composition to form ZrB_2 and SiC by reaction (1).

The additive contents were 30, 40, and 50 wt% of the total weight (termed ZS30, ZS40, ZS50, respectively), which corresponded to 12.5, 16.1, and 20.8 wt% of SiC after reaction (1). On the other hand, 0, 10, and 20 wt% of nano-SiC powder (T-1, Sumitomo-Osaka Cement Co., Tokyo, Japan, d_{50}: 30 nm, β-SiC, O: 0.45 wt%, C: 3.73 wt%) was mixed with the ZrB_2 powder (termed SC0, SC10, and SC20, respectively) to compare the microstructure and sintering behavior.

The raw materials were mixed using a WC jar and balls for 6 h using a high-energy ball mill (M-8000, Spex Sample Prep., Metuchen, NJ, ball:powder = 10:1, 5 g per batch). After milling, the powder mixtures were granulated through a metallic sieve with a #150 mesh size and were loaded into a graphite mold (inner diameter 10 mm).

The powder mixtures were densified using a spark plasma sintering apparatus (SPS; Dr-Sinter 4000, SPS Syntax, Kamagawa, Japan) at 1400–1500 °C for 30–60 min under 120 MPa pressure in vacuum (heating rate: 50 °C/min). The heating process was controlled using a monochromatic optical pyrometer that was focused on a hole at the side of the graphite mold. The sintering shrinkage of the specimen was analyzed by measuring the displacement of the lower electrode (resolution 0.01 mm) which was connected to a computer to log the shrinkage curves.

Specimens of 2 × 10 × 25 mm size were obtained, which were machined into 1.5 × 2 × 25 mm bars. A 4-point bending test was performed using 5 specimens per condition according to the ASTM standard.[19] After grinding and polishing the surface of the sintered specimens, the bulk densities were measured using Archimedes' method. The theoretical densities of ZrB_2, SiC, $ZrSi_2$, B_4C, and C to calculate the volume shrinkage by reaction (1) and relative density were 6.09, 3.2, 4.88, 2.52, and 2.27 g/cm^3, respectively.[20] The phase identification and microstructure of the sintered specimens were analyzed by X-ray diffractometry (XRD; D-Max2200, Rigaku Co., Tokyo, Japan) using Cu $K_{\alpha 1}$ radiations (wave length: 1.54056 Å) and scanning electron microscopy (SEM; JSM-6700F, Jeol, Tokyo, Japan), respectively. An image analysis program (Nano measurer, China) was used to precisely measure the grain size. At least 200 grains per specimen were measured for the determination of the average grain size.

III. RESULTS AND DISCUSSION

A. Properties of the powders

Figure 1(a) shows the XRD data of the $ZrSi_2$–B_4C–C powder mixture after HEBM. The decrease of peak intensity and the broadening of the peaks indicated the ultrafine particle size of the $ZrSi_2$–B_4C–C mixture after

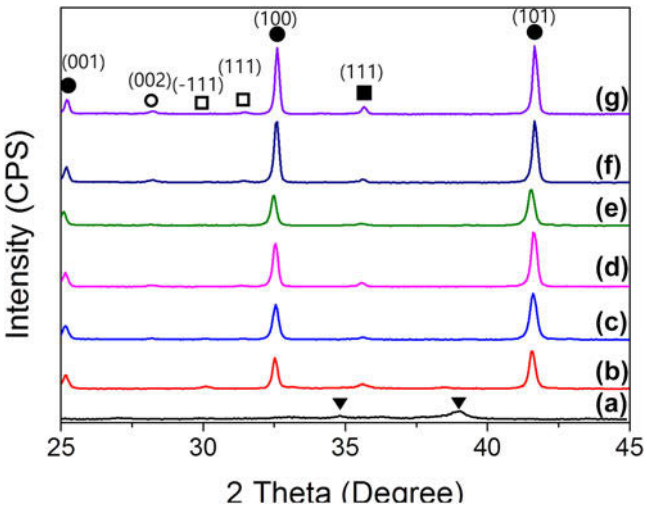

FIG. 1. XRD data of sintered ZrB_2–SiC composites. (a) $ZrSi_2$–B_4C–C powder mixture after HEBM, (b) ZS40, 1200 °C, (c) ZS40, 1400 °C, (d) ZS50, 1450 °C, (e) SC20, 1450 °C, (f) ZS40, 1500 °C, and (g) ZS40, 1650 °C (▼: $ZrSi_2$, ■: ZrB_2, ●: SiC, □: ZrO_2, ○: graphite).

high-energy milling. The initial particle sizes of ZrB_2 and $ZrSi_2$ were 2.12 and 27.5 μm, while the average particle size of the $ZrSi_2$–B_4C–C mixture after HEBM was calculated to be 8 nm by the Sherrer equation. Carbon black was not detected by XRD because of its amorphous state. The peaks of SiC were not identified after milling, which indicated that reaction (1) did not actively occur during the HEBM process.

Figure 2 shows the SEM images of the powders after HEBM and after heating at 1200 °C. Fine and homogeneously intermixed particles were observed after HEBM [Fig. 2(a)]. Although the primary particle size after HEBM was measured to be 8 nm by X-ray analysis, the average particle size analyzed by the image analyzer was 310 nm because the particles were strongly agglomerated by cold welding during the milling process. Cold welding is a general expression in the field of mechanical alloying. During the high-energy milling of powder, the powders form a very hard agglomeration by the mechanical energy even at room temperatures.

After heating at 1200 °C, the formation of phases with different sizes and colors was clearly identified [Fig. 2(b)]. The EDS data indicated that the particles larger than 300 nm in size were ZrB_2. Most of the synthesized SiC particles were round in shape and were smaller than 100 nm. Although $ZrSi_2$ has the molecular-level homogeneity of Zr and Si, the size of ZrB_2 particles was larger than that of SiC particles after reaction (1). The result indicated that the growth rate of ZrB_2 particles is faster than that of SiC particles.[17]

B. Densification behavior

Table I shows the effect of the nano-SiC powder or $ZrSi_2$–B_4C–C additive contents on the sintered density. The relative density of the crushed ZrB_2 (SC0) was 95.5% after sintering at 1450 °C under 120 MPa pressure. The enhanced densification of the milled ZrB_2 was caused by the strong decrease of the particle size to about 8 nm and a consequent increase of the rearrangement of the particles and the driving force for densification.[12] In addition, the imperfections in the crushed powder promoted the deformation of the particles at relatively low temperatures under high pressure (120 MPa).[14]

The densification of the milled ZrB_2 was clearly suppressed when adding nano-SiC powder (Table I). This result was inconsistent with those reported by Zamora et al. where the addition of SiC promoted the densification of ZrB_2 after HEBM due to a borosilicate glass which was formed during the process.[21] (Fig. 5) Figure 4 shows the polished cross-section of SC20 after sintering at 1850 °C. The high sintering temperature was required to obtain dense specimens for the analysis of the microstructure. The nano-SiC particles were strongly aggregated. The aggregated SiC was not fully densified in spite of the high sintering temperature and pressure. Nadeau et al. reported that high temperature and pressure (2100 °C, 2 GPa) were simultaneously required for the densification of high-purity SiC.[22]

In contrast to the detrimental effect of nano-SiC on densification, the $ZrSi_2$–B_4C–C system did not suppress the densification of ZrB_2. The relative densities of ZS30–ZS50 were 88.9–94.2% after sintering at 1400 °C for 1 h,

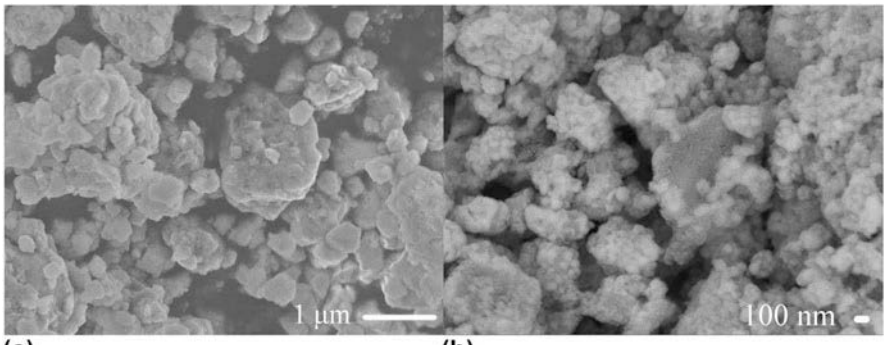

FIG. 2. Morpholigy of ZS40 powders (a) after mixing and (b) after heating at 1200 °C.

TABLE I. Relative density and flexural strength of specimens sintered at various conditions under 120 MPa pressure in vacuum.

Temperature (°C)	Time (min)	R.D. (%) (flexural strength, MPa)					
Abbreviation		SC0	SC10	SC20	ZS30	ZS40	ZS50
1400	60	91.0	...	...	91.4	88.9	94.2 (309 ± 35)
1450	60	96.5	88.3	78.2	92.5	99.5	98.5
1500	30	...	...	...	98.5 (334 ± 42)	100 (353 ± 55)	96.2 (354 ± 86)

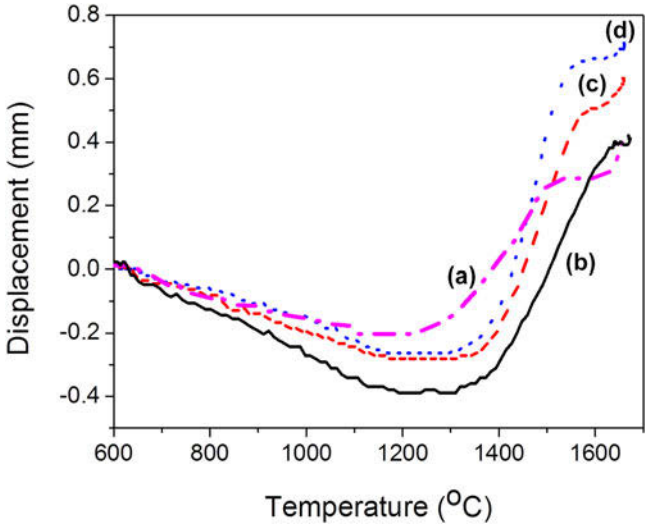

FIG. 3. Shrinkage behavior during sintering at 1650 °C for 5 min at a pressure of 120 MPa. (a) SC0, (b) ZS30, (c) ZS40 and (d) ZS50.

which were similar with that of SC0 (91.0%). The densification of ZS40 and ZS50 was mostly completed at 1450 °C (Table I). ZS40 and ZS50 contained different amounts of the additives (40 and 50 wt% of total weight). In all cases, the heating rate was fixed to 50 °C/min.

Figure 3 shows the sintering shrinkage behavior. The shrinkage became more distinct when the additive content increased because of the volume shrinkage of 11.2% by reaction (1). In all cases, the shrinkage stopped below 1650 °C, indicating that the densification was mostly completed during heating. The shrinkage curves could be divided into three stages.

The displacement data in Fig. 3 did not precisely reflect the sintering behavior of the powder because the data were obtained from the displacement of the lower electrode of the SPS (resolution 0.01 mm). The expansion below 1000 °C was the summation of the thermal expansion of the powder, graphite punches, and graphite spacers.

The expansion stopped when the first sintering stage started because the thermal expansion of the punches was compensated by the shrinkage of the powder. The onset temperatures of the first sintering stage were 1100, 1192, 1173, 1165 °C for SC0 and ZS30–ZS50, respectively. According to the results from the XRD analysis (Fig. 1), reaction (1) was mostly completed at this stage. The melting temperature of $ZrSi_2$ is 1620 °C, and the material can be densified above 1100 °C by plastic deformation.[15,23] However, the deformation of $ZrSi_2$ did not have a strong effect on the densification of the ZS systems because the silicide mostly transformed into ZrB_2 and SiC below the temperature of the first stage. The reaction was reported to occur rapidly once started.[17] The oxides which formed on the surface of $ZrSi_2$ prevent the reaction to occur at low temperatures. Once the oxide became unstable during heating, the reaction was reported to be mostly completed within a few seconds. In addition, the first stage was observed in SC0 which did not contain $ZrSi_2$. Also, the onset temperature of the first sintering stage is too low to induce the densification of ZrB_2 and SiC by thermal diffusion.

During SPS, the pressure at the contact point between the particles is amplified by the applied pressure until the local pressure exceeds the yield strength at the processing temperature.[24] In addition, at the initial stage of SPS, the small contact point between the particles concentrates the current, which can induce the local increase of temperature and electromigration.[25] Electromigration usually occurs at current densities over 1000 A/cm^2 and when the powder has a relatively low electrical resistivity (resistivity of HfC: 60×10^6 Ω cm at 300 K).[26] The local increase of pressure and temperature as well as electromigration at the contact point promoted the deformation and rearrangement of the particles at the first stage. The rearrangement was reported to be promoted by the ultrasmall particle size (~10 nm) produced by the high-energy milling.[14]

The onset temperatures of the second stage for SC0 and ZS30–ZS50 were 1214, 1310, 1315, and 1290 °C, respectively, where the shrinkage began to occur. The results indicated that the densification of the second stage was initiated by that of the ZrB_2 pre-treated by HEBM because the onset shrinkage temperature of SC0 was the lowest among the tested specimens. The $ZrSi_2$–B_4C–C additives increased the onset shrinkage temperature of the finely crushed ZrB_2 powder. However, the onset temperature of shrinkage of the ZS systems decreased slightly when the additive content increased. The second stage is a sintering regime where the accelerated densification occurred and the pore distribution changes from open porosity to closed porosity.

Particle size has an important effect on the solid-state sintering in terms of temperature. The sintering temperature was reported to decreases with particle size, especially when the size was below 30 nm.[27] The sintering of tungsten was reported to start at 825 °C for 31 nm particles, while the behavior occurred at 625 °C when using 9 nm powder.[27] Consequently, the formation of ultrafine particles (8 nm) by HEBM is one of the major reasons for the low temperature sintering of the ZrB_2–$ZrSi_2$–B_4C–C powder.

At the beginning of the significant shrinkage, the densification of ZS was effectively promoted by the fine particles formed by reaction (1). The crystal size refinement and homogeneous mixing of the starting powders by HEBM increased the reaction area and thus promoted reaction (1). During the reaction, ultrafine ZrB_2 and SiC phases nucleated at the interface of $ZrSi_2$ and C.[17] Growth of the new phases was suppressed by SPS

because of the fast heating/cooling rate and the low densification temperature.

The refinement of ZrB_2 grains after densification can also be explained by Zener effect.[28] The ultrafine secondary phase, which is placed at the grain boundaries of the matrix phase, exerts a drag force against the boundary movement and causes the inhibition of grain growth. Liu et al. reported that nano-SiC particles suppressed the growth of ZrB_2 grains from 7.5 to 2 μm.[29] ZS40 and ZS50 became highly dense after the isothermal heating at 1450 °C for 60 min under 120 MPa pressure. The average grain size of ZrB_2 in the ZS decreased with increasing the additive content, which will be explained in the following paragraphs. The densification of ZS was improved when the additive content increased. The promotion of Zener effect and consequent suppression of grain growth is believed to be the main reason because the deformation of $ZrSi_2$ did not strongly induce the densification of the ZS system.

The shrinkage rate decreased rapidly at the third stage, indicating that the densification was mostly completed during heating. The third stage started at 1520, 1640, 1592, and 1572 °C for SC0 and ZS30–ZS50, respectively. The result indicated that the densification of the powder mixture was mainly performed by that of the crushed ZrB_2. Consequently, the densification mechanism of the ZrB_2–$ZrSi_2$–B_4C–C system is considered to be solid-state sintering like the case of high-energy milled ZrB_2.[12,14]

Based on the above discussion, the densification mechanism of the ZrB_2–SiC composites prepared using $ZrSi_2$, B_4C, and C powder mixtures could be proposed as follows. The deformation of $ZrSi_2$ and the reaction between $ZrSi_2$, B_4C, and C did not result in the significant densification. The densification became distinct after the reaction was completed. Ultrafine and homogeneously distributed ZrB_2 and SiC particles which were introduced by HEBM and R-SPS effectively promoted the densification.

Table I summarized the 4-point bending strength of the composites. The relative high porosity of ZS50 sintered at 1400 °C induced the low strength of the specimens compared to those sintered at 1500 °C. A maximum bending strength of 354 MPa was obtained.

C. Phase compositions and microstructures after densification

Figures 1(b)–1(g) show the XRD data of the ZS and SC systems after heating at different temperatures. In ZS, the peaks of $ZrSi_2$ (major peak: 38°) and B_4C mostly disappeared and the formation of SiC by reaction (1) was identified after heating at 1200 °C [Fig. 1(b)].

The phase formation did not strongly change up to 1450 °C [Figs. 1(c)–1(e)]. The results indicated that the additive system was mostly consumed by reaction (1) below the onset temperature of shrinkage (≥1165 °C) because the Gibbs free energy of reaction (1) is negative at and above room temperature. Reaction (1) was reported to occur at and above 860 °C when $ZrSi_2$–B_4C–C powders were strongly mixed by HEBM.[17] The reaction between $ZrSi_2$–B_4C–C was reported to occur rapidly once started.[17] The oxides formed on the surface of $ZrSi_2$ prevent the reaction from occuring at low temperatures. Once the oxide became unstable at high temperatures, the reaction was reported to be completed within a few seconds.

The ratio of the main peak intensity of ZrB_2 and SiC was similar between ZS50 and SC20 which contained similar amounts of SiC [20.8 versus 20 wt%, Figs. 1(d) and 1(e)]. The result also indicated that $ZrSi_2$ was mostly consumed to form ZrB_2 and SiC during densification.

The intensity of the ZrB_2 peaks increased and the width decreased when the sintering temperature was at and above 1500 °C [Figs. 1(f) and 1(g)] because the grain coarsening became distinct at 1500 °C.

In both the ZS and SC systems, the presence of ZrO_2, which was formed during the storage and crushing of ZrB_2 powder, was evident in the sintered specimens. The amorphous zirconium hydroxides on the surface of the raw powders were crystallized during densification. B_4C and C in the ZS systems can effectively remove ZrO_2 by carbo–boro thermal reduction;

$$2ZrO_{2(s)} + B_4C_{(s)} + 3C_{(s)} \rightarrow 2ZrB_{2(s)} + 4CO_{(g)} \quad , \quad (2)$$

$$7ZrO_{2(s)} + 5B_4C_{(s)} \rightarrow 7ZrB_{2(s)} + 3B_2O_{3(l,g)} + 5CO_{(s)} \quad , \quad (3)$$

$$ZrO_{2(s)} + B_2O_{3(l)} + 5C_{(s)} \rightarrow ZrB_{2(s)} + 5CO_{(g)} \quad . \quad (4)$$

However, the reduction reactions did not actively occur because reactions (2)–(4) have negative Gibbs free energy above 1424, 1218, and 1509 °C at a standard condition while the value of reaction (1) is negative at room temperature.[16] Consequently, B_4C and C were preferentially consumed by reaction (1) before reactions (2)–(4) can actively occur.

Figure 4 displays the microstructure of the ZS systems. The amount of SiC, depicted as dark grains, in ZS50 was larger than that of ZS30 [Figs. 4(a) and 4(b)]. The average grain size of ZrB_2 and SiC in ZS30 was 352 and 81 nm after sintering at 1400 °C for 60 min, whereas the values changed to 213 and 90 nm in ZS50. By the application of the HEBM and $ZrSi_2$ additive which has molecular-level homogeneity between Zr and Si, dense ZrB_2–SiC composites with fine and homogeneously distributed ZrB_2 and SiC grains were successfully fabricated. The small grain size and homogeneous distribution

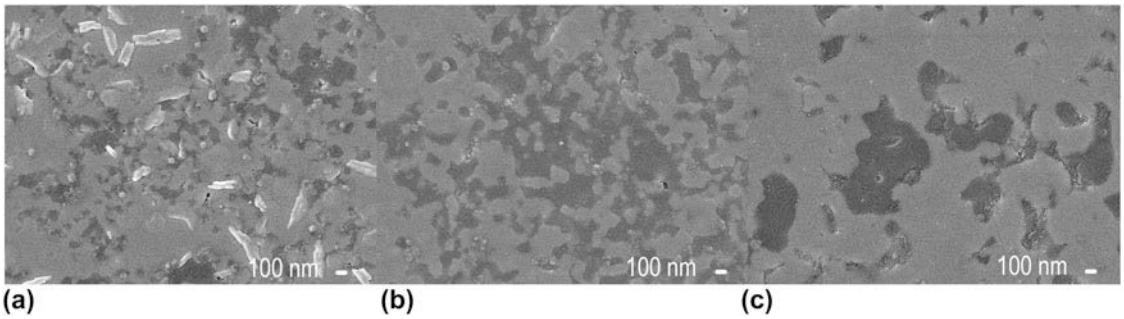

FIG. 4. Polished cross-section of the specimens after sintering for 1 h under 120 MPa pressure in vacuum. (a) ZS30, 1400 °C, (b) ZS50, 1400 °C, and (c) ZS50, 1500 °C.

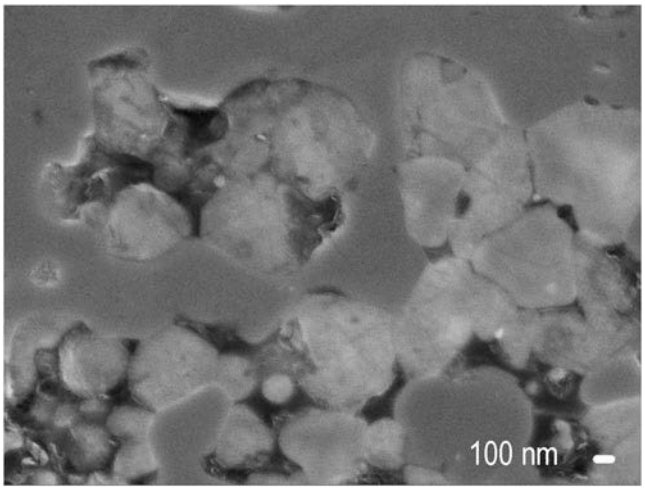

FIG. 5. Polished cross-section of SC20 after sintering at 1850 °C for 1 h under 120 MPa pressure in vacuum.

of the ZrB_2 and SiC phases are related with the strong mixing and efficient size refinement of raw powders by HEBM and low sintering temperature by R-SPS under high pressure. (Fig. 5).

Two reasons are considered to explain the difference in the grain size between ZrB_2 and SiC after densification. First, the growth of ZrB_2 grains was faster than that of SiC, which was also observed during the synthesis of ZrB_2–SiC powder mixture by the reaction of $ZrSi_2$–B_4C–C.[17] Second, a part of the coarse ZrB_2 powder did not get crushed below 200 nm or intermixed with the additives after HEBM.

The agglomeration and growth of SiC grains occurred when the sintering temperature increased to 1500 °C [Fig. 4(c)], which result was in accordance with that of the XRD [Figs. 1(f) and 1(g)].

IV. CONCLUSIONS

The ZrB_2–SiC nanocomposites were successfully fabricated by the R-SPS at 1450 °C. The ultrafine particle size (~10 nm) caused by HEBM of ZrB_2 promoted the rearrangement of particles and the densification at the first and second stage of sintering. The formation of ZrB_2 and SiC by the reaction of $ZrSi_2$–B_4C–C was mostly completed at 1200 °C. The resultant nano-SiC did not inhibit the densification of ZrB_2. The sizes of SiC grains were 100–300 nm and the phases were homogeneously distributed because of the molecular-level homogeneity of Zr and Si in $ZrSi_2$ and the high-energy milling of the raw powders. By contrast, the nano-SiC powder which was added to the crushed ZrB_2 powder formed strong aggregation and suppressed the densification of ZrB_2–SiC composites. The deformation of $ZrSi_2$ and the reaction between $ZrSi_2$, B_4C, and C did not strongly promote the densification. Instead, ultrafine and homogeneously distributed ZrB_2 and SiC particles prepared by HEBM and R-SPS effectively promoted the densification. A maximum bending strength of 354 MPa was obtained after sintering the ZrB_2–SiC composites at 1500 °C.

ACKNOWLEDGMENT

This research was supported by the National Research Council of Science & Technology (NST) grant by the Korea government (MSIP) (No. PCS-17-09-KIMS).

REFERENCES

1. D. Sciti, L. Pienti, D.D. Fabbriche, S. Guicciardi, and L. Silvestroni: Combined effect of SiC chopped fibers and SiC whiskers on the toughening of ZrB_2. *Ceram. Interfaces* **40**, 4819 (2014).
2. E.W. Neuman, G.E. Hilmas, and W.G. Fahrenholtz: Mechanical behavior of zirconium diboride–silicon carbide ceramics at elevated temperature in air. *J. Eur. Ceram. Soc.* **33**, 2889 (2013).
3. L. Silvestroni and D. Sciti: Densification of ZrB_2–$TaSi_2$ and HfB_2–$TaSi_2$ ultra-high-temperature ceramic composites. *J. Am. Ceram. Soc.* **94**, 1920 (2011).
4. J. Yin, H. Zhang, Y. Yan, and Z. Huang: High toughness in pressureless densified ZrB_2-based composites co-doped with boron–titanium carbides. *Scr. Mater.* **66**, 523 (2012).
5. X.G. Wang, W.M. Guo, Y.M. Kan, and G.J. Zhang: Hot-pressed ZrB_2 ceramics with composite additives of Zr and B_4C. *Adv. Eng. Mater.* **12**, 893 (2010).

6. G.J. Zhang, Z.Y. Deng, N. Kondo, J.F. Yang, and T. Ohji: Reactive hot pressing of ZrB_2–SiC composites. *J. Am. Ceram. Soc.* **83**, 2330 (2000).
7. J.W. Zimmermann, G.E. Hilmas, W.G. Fahrenholtz, F. Monteverde, and A. Bellosi: Fabrication and properties of reactively hot pressed ZrB_2–SiC ceramics. *J. Eur. Ceram. Soc.* **27**, 2729 (2007).
8. H.L. Wang, S.H. Lee, and L. Feng: The processing and properties of (Zr, Hf)B_2–SiC nano-structured composites. *J. Eur. Ceram. Soc.* **34**, 4105 (2014).
9. L. Feng, S.H. Lee, H.L. Wang, and H.S. Lee: Nanostructured HfC–SiC composites prepared by high-energy ball-milling and reactive spark plasma sintering. *J. Eur. Ceram. Soc.* **36**, 235 (2016).
10. W.W. Wu, G.J. Zhang, Y.M. Kan, P.L. Wang, K. Vanmeensel, J. Vleugels, and O. Van der Biest: Synthesis and microstructural features of ZrB_2–SiC-based composites by reactive spark plasma sintering and reactive hot pressing. *Scr. Mater.* **57**, 317 (2007).
11. W.W. Wu, G.J. Zhang, Y.M. Kan, and Y. Sakka: Synthesis, microstructure and mechanical properties of reactively sinterd ZrB_2–SiC–ZrN composites. *Ceram. Interfaces* **39**, 7273 (2013).
12. C.A. Galán, A.L. Ortiz, F. Guiberteau, and L.L. Shaw: High energy ball milling of ZrB_2 in the presence of graphite. *J. Am. Ceram. Soc.* **93**, 3072 (2010).
13. L.S. Walker, W.R. Pinc, and E.L. Corral: Powder processing effects on the rapid low-temperature densification of ZrB_2–SiC ultra-high temperature ceramic composites using spark plasma sintering. *J. Am. Ceram. Soc.* **95**, 194 (2012).
14. S.H. Lee, H.C. Oh, J.H. Kim, and H.D. Kim: Low temperature densification of ZrB_2 by the mechanical pre-treatment of particles. *J. Ceram. Soc. Jpn.* **121**, 480 (2013).
15. S. Guo, T. Nishimura, and Y. Kagawa: Low-temperature hot pressing of ZrB_2-based ceramics with $ZrSi_2$ additives. *Int. J. Appl. Ceram. Technol.* **8**, 1425 (2011).
16. O.N. Grigoriev, B.A. Galanov, V.A. Kotenko, S.M. Ivanov, A.V. Koroteev, and N.P. Brodnikovsky: Mechanical properties of ZrB_2–SiC($ZrSi_2$) ceramics. *J. Eur. Ceram. Soc.* **30**, 2173 (2010).
17. S.H. Lee, S.Y. Choi, and H.D. Kim: ZrB_2–SiC nano-powder mixture prepared using $ZrSi_2$ and modified SPS. *J. Am. Ceram. Soc.* **96**, 1051 (2013).
18. W.M. Guo and G.J. Zhang: Oxidation resistance and strength retention of ZrB_2–SiC ceramics. *J. Eur. Ceram. Soc.* **30**, 2387 (2010).
19. ASTM C 1161, Test method for flexural strength of advanced ceramics at ambient temperature.
20. *CRC Handbook of Chemistry and Physics*, 89th ed., D.R. Lide, ed. (CRC Press, Boca Raton, FL, 2008); pp. 4-15–4-97.
21. V. Zamora, A.L. Ortiz, F. Guiberteau, and M. Nygren: On the enhancement of the spark-plasma sintering kinetics of ZrB_2–SiC powder mixture subjected to high energy co-ball-milling. *Ceram. Interfaces* **39**, 4191 (2013).
22. J. Nadeau: Very high pressure hot pressing of silicon carbide. *Am. Ceram. Soc. Bull.* **52**, 170 (1973).
23. T. Nakano, Y. Omomoto, K. Hagihara, and Y. Umakoshi: Plastic deformation behavior and operative slip systems of $ZrSi_2$ single crystals with C49 type of structure. *Scr. Mater.* **48**, 1307 (2003).
24. R.M. German: *Sintering: From Empirical Observations to Scientific Principles* (Elsevier, Waltham, MA, 2014); pp. 309–326.
25. D.R. Campbell and H.B. Huntington: Thermomigration and electromigration in zirconium. *Phys. Rev.* **179**, 609 (1969).
26. *CRC Materials Science and Engineering Handbook*, 3rd ed., J.F. Shackelford and W. Alexander, eds. (CRC Press, Boca Raton, FL, 2001); pp. 956–958.
27. R.M. German: *Sintering Theory and Practice* (John Wiley & Sons, Inc., New York, NY, 1996); pp. 73–74.
28. S-K.L. Kang: *Sintering: Densification, Grain Growth, and Microstructure* (Elsevier Butterworth-Heinemann, New York, NY, 2005); pp. 45–156.
29. Q. Liu, W. Han, and J. Han: Influence of SiC_{np} content on the microstructure and mechanical properties of ZrB_2–SiC nanocomposites. *Scr. Mater.* **63**, 581 (2010).